A PATH LOSS FORMULATION FOR WIRELESS APPLICATIONS CONSIDERING TERRAIN EFFECTS FOR URBAN ENVIRONMENTS

Leonard Piazzi and Henry L. Bertoni

Center for Advanced Technology in Telecommunications
Polytechnic University
Brooklyn, NY 11201

Abstract — This study examines propagation over buildings when the buildings are located on terrain features (hills). The buildings, which are represented by a series of absorbing half-screens, are assumed to lie in rows that are equally spaced along parallel streets, with the streets running perpendicular to the terrain slope. Numerical results are obtained using successive repetition of the Kirchhoff-Huygens approximation. A phenomenological model based on ray optics for diffraction over a smooth surface is proposed as a way to interpret the numerical results. The dependence of model coefficients on terrain parameters are obtained from the numerical results.

I. INTRODUCTION

Away from the high rise core of the city, base station antennas for mobile radio are typically above or near to the rooftops of the surrounding buildings. For flat terrain propagation has been modeled by multiple forward diffraction past rows of buildings [1]-[4]. In order to model the path loss for the case of buildings on rolling hills, we assume the streets, and hence the rows of buildings are oriented perpendicular to the plane of curvature of the hills, as shown in side view in Figure 1, which is also assumed to be the plane of propagation. For mobiles located on the up slope of hills visible to the base station, as indicated by position ① in Figure 1, the path loss can be found using the theory previously derived for flat terrain if the angle of incidence on the rooftops, α, in that theory is replaced by the angle α_l to the local tangent plane, as indicated in Figure 1. This method is equivalent to using an effective antenna height, as discussed by Lee [5]. However, these results do not apply when terrain shadowing occurs, such as at locations ② and ③ in Figure 1.

We first consider cylindrical and sinusoidal terrain variation. In order to treat the forward diffraction, each row of buildings is modeled as an absorbing knife-edge. The field dependence above a knife-edge is given as a function of the field above the previous knife-edge, and a direct numerical solution to the Kirchhoff-Huygens approximation is performed. Utilizing this method, over 100 knife-edges may be considered with acceptable computation times. The results we obtain indicate that a cylindrical representation for the hills in the terrain profile must be used, as opposed to single knife edge at the hill peak, or else the resultant path loss values are too optimistic, particularly in the deep shadow of the hill.

The numerical technique discussed above is too cumbersome to be incorporated into a cellular planning tool. We therefore interpret the numerical results in terms of ray optics in order to obtain a compact approximation. This interpretation is similar to the creeping ray formulation for diffraction over a smooth circular cylinder. The field strength along the creeping ray decreases exponentially with arc length traveled on the surface of the cylinder, with a decay factor that depends on the radius of the cylinder. Excitation of the creeping ray by a source is described by an excitation coefficient and subsequent radiation into space by a launch coefficient, which are also dependent upon the cylinder radius [6],[7].

II. MODELING TERRAIN EFFECTS

Figure 1 illustrates in cross-section rows of houses that are equally spaced along parallel streets, with the streets running perpendicular to the slope of the hills. In this example the transmitting antenna is placed at the maximum height of the terrain plus house height. For area ① in Figure 1, the path loss may be determined using the Walfisch-Ikegami model, accounting for terrain slope by means of the local angle α_l. The path loss ratio between isotropic antennas in watts received/watts transmitted is then given by

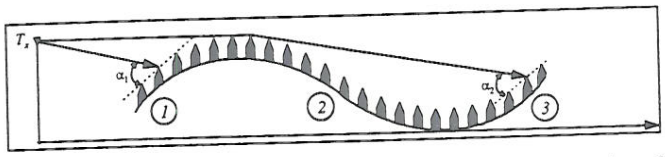

Figure 1: Rows of houses on rolling terrain. For areas 1 and 3 the angle with the local tangent may be used to determine the path loss.

$$P_L = \left(\frac{\lambda}{4\pi R}\right)^2 P_d \left[Q(\alpha_l)\right]^2 \qquad (1)$$

The factor P_d is the diffraction loss from the last rooftop before the mobile down to the street, and $Q(\alpha_l)$ is the multiple screen diffraction loss, which can be found from the polynomial approximation [8]

$$Q = 3.502 g_p - 3.327 g_p^2 + 0.962 g_p^3 \qquad (2)$$

VTC '98

over the range $0.01 < g_p < 1.00$. The dimensionless parameter g_p is given by

$$g_p = \alpha\sqrt{d/\lambda} \tag{3}$$

where d is the separation between rows of buildings. For $g_p > 1.0$, the previous rows of buildings have almost no effect and $Q \approx 1.0$.

A. *Isolated Cylindrical Hill*

To facilitate the description of the field variation in regions ② and ③ of Figure 1 we first characterize the terrain variation as that of an isolated cylindrical hill. To determine the effects of an isolated hill we make use of the terrain profile illustrated in Figure 2. The height of the hill plus building height as a function of the distance x from the peak of the hill is given by

$$y = \sqrt{R_h^{\,2} - x^2} - y_o + h_b \tag{4}$$

where R_h is the hill radius and $y_o > 0$ is the distance that the center of curvature lies below the flat portion of the terrain.

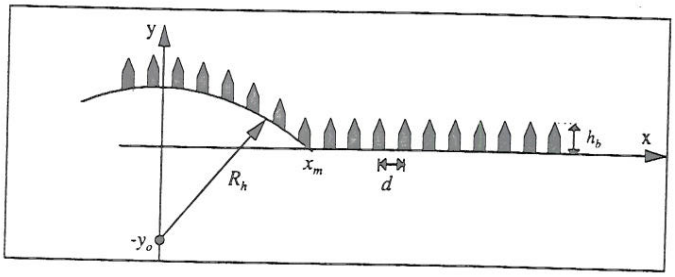

Figure 2: Illustration of houses on an isolated cylindrical hill having radius of curvature R_h.

The maximum slope, or *grade*, of the hill occurs at x_m and is given by $grade = -dy/dx$. Knowing the grade and the horizontal distance x_m from the peak to the foot of the hill, the equivalent hill radius R_h is

$$R_h = x_m\sqrt{1 + (1/grade)^2} \tag{5}$$

This expression is used to choose realistic values for R_h in carrying out the numerical evaluation discussed below. Examination of terrain elevation maps, suggests that the radius of curvature of rolling terrain is typically much larger than 1 km.

B. *Numerical Evaluation of the Line Source Fields*

Since the Fresnel zones in the UHF band out to a few km are narrow, it is reasonable to use a two dimensional model by assuming the geometry in Figure 2 to be uniform along z. Propagation oblique to the street grid can be accounted for by using the terrain profile and spacing d between rows of buildings as seen in the vertical plane containing the transmitter and receiver. On flat terrain this approach gives reasonable accuracy, as compared to measurements for planes making angles as much as 60° to the street grid [9]. With the assumption of a two dimensional model, the excess path loss due to the rows of buildings and terrain will be the same for a point source and for the fields radiated by a line source parallel to z. Propagation of the line source fields from the plane of one screen to the next is carried out numerically using the Kirchhoff-Huygens approximation as in [1]. However, truncating the integration at a finite value of y does not follow the approach used in [1], since in that study the window function was tailored to the specific case of an incident plane wave field directed down towards the screens. In this manner we can account for diffraction past 100 or more screens, and therefore, can account for houses on sinusoidal and cylindrical terrain.

III. *Numerical Results for a Cylindrical Hill*

The half screens used to represent the rows of buildings for a typical case are shown in Figure 3. The houses are 7 m high and the row separation d, is 50 m. In this figure the base of the hill occurs at x_m = 1000 m, and the maximum *grade* is 10%, so that the hill radius is 10.0 km, and its maximum height is 50 m. The transmitting antenna is located at x_s = -1000 m, and at a height y_s equal to the maximum screen height of 57 m.

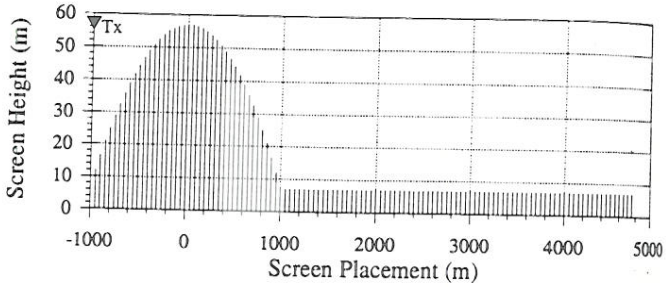

Figure 3: Screen profile for typical hill radius parameters.

The results of the numerical evaluation for 900 MHz are shown in Figure 4 for the screen profile given in Figure 3. The field strength in dB has a nearly linear variation on the back-side of the hill (0m - 1000m), where diffraction from rooftop-to-rooftop occurs over a cylindrical-like surface. The minimum field strength value occurs at 1000 m, which is the base of the hill. After this point the field strength increases out to about 3500 m, after which it decreases slowly. The same type of variation is found for all choices of hill radius R_h, row separation d and frequency, and can be modeled by a creeping wave.

The rise in field strength after the hill is attributable to the fact that the diffracted rays are now launched from points higher up on the hill, and thus experience less diffraction loss before being launched. Immediately after the hill the foregoing effect more than compensates for the usual inverse distance dependence. However, for the rooftops far from the hill the rays are launched from near to the top of the hill so

:hat the inverse distance dependence causes a decrease in signal strength.

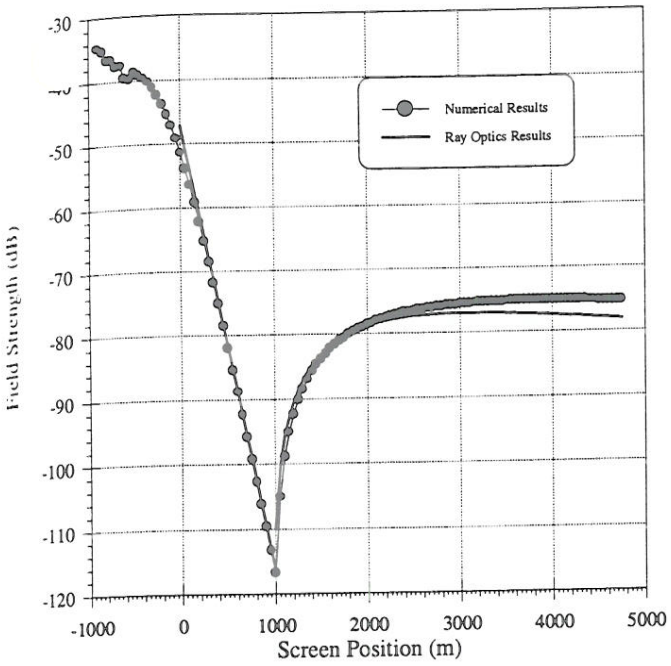

Figure 4: Field strength versus screen position distance for the screen profile shown in Figure 3.

IV. Creeping Rays for Non-LOS Rooftops

creeping ray representation for the field diffracted by a circular cylinder is shown in Figure 5 for points outside of the transition region centered on the shadow boundary. Unlike the case of diffracting from absorbing screens, for which the TE and TM polarizations have the same path loss, in the case of a conducting cylinder the two polarizations behave differently.

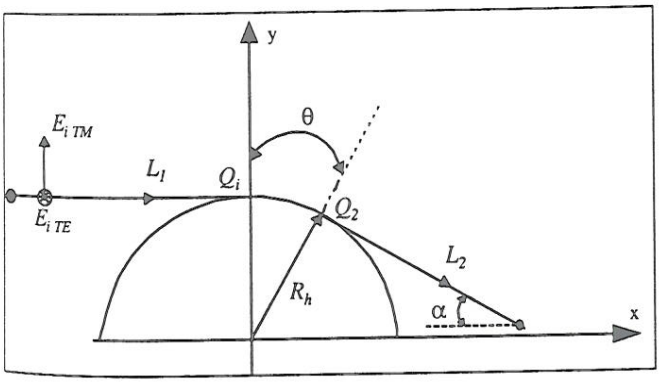

Figure 5: Diffraction by a circular cylinder.

The asymptotic representation for the creeping ray field at observation points behind the cylinder for an incident plane or cylindrical wave is [6]

$$E \sim E_i(Q_i)e^{-jkR_h}\frac{e^{-jkL_2}}{\sqrt{2\pi\, kL_2}}\cdot\sum_{p=1}^{\infty}D_p^{m,e}(R_h)\exp\left(-\psi_p^{m,e}\theta\right) \qquad (6)$$

Here $E_i(Q_i)$ is the incident field at the excitation point, L_2 is the distance from the launch point, and the coefficients $D_p^{m,e}$, and $\psi_p^{m,e}$ are functions of hill radius and frequency. The attenuation constants ψ_p^m for TM polarization and ψ_p^e for TE polarization are given by

$$\psi_p^{m,e} = a_p^{m,e}\left(\frac{kR_h}{2.0}\right)^{1/3}e^{j\pi/6} \qquad (7)$$

The first few values of $a_p^{m,e}$ for the TE polarization are $a_1^e = 2.338$, $a_2^e = 4.088$, $a_3^e = 5.521$.

Near the shadow boundary where θ is small, the sum is slowly convergent, while deeper into the shadow, where the higher terms in the sum have decayed more rapidly, only the $p = 1$ term is important. The values of ψ_p^m for TM polarization are smaller than those for TE polarization.

A. Ray Optics for the Backside of the Hill

In representing the results obtained from the numerical integration, we retain only the first term in the creeping ray representation. To find the attenuation coefficient ψ, we examine the field at the top of the screens on the back side of the hill before the ray is launched. The field amplitude at these points due to a line source at a distance L_1 from the top of the hill is assumed to be of the form

$$\left|E(x_n,h_n)\right| = \frac{1}{\sqrt{L_1}}D_H e^{-\psi\theta} \qquad (8)$$

The coefficients D_H and ψ are determined from the multiple integration results, as shown in Figure 4, by fitting the numerical values at the farthest end of the hill. Because the values of x_n on the back side of the hill are much less than the hill radius, the angle $\theta \approx x_n/R_h$ so that (8) predicts a linear variation of the field, in dB with x_n. In Figure 4 the variation with x_n of the field strength in dB at the top of the screens, as obtained from the multiple integration, is seen to be nearly linear indicating the dominance of the $p = 1$ term in (6). The deviation from linearity reflects the importance near the shadow boundary of the terms in (6) having $p > 1$.

Figure 4 shows a comparison of the field amplitude on the back side of the hill obtained from the approximation of (8) with the field computed by numerical integration. The location of the minimum field strength value (1000 m) is seen from (8) to result from the creeping ray that travels the greatest distance around the cylinder. As we approach the peak of the hill from the back side using the ray optics method the result is more optimistic than the numerical integration result. Had more terms of the type shown in (6) been used to fit the computed results, a better fit would have been obtained close to the peak of the hill.

The values of ψ found by fitting the numerical results for various R_h,, d, and λ are found to be given by the simple approximation

0-7803-4320-4/98/$5.00 © 1998 IEEE

$$\psi = 2.02\left(\frac{\pi R_h}{\lambda}\right)^{1/3} - 1.04\sqrt{\frac{d}{\lambda}} \qquad (9)$$

which reduces to the theoretical diffraction result over a smooth hill for TE polarization [7] when $\sqrt{d/\lambda} = 0$. The excitation coefficient, D_H in (8), is found from the fit to the numerical results, and is approximated by the expression

$$\ln(D_H) = 4.04 + (-0.576 + 0.059\ln(d/\lambda))\ln(R_h/\lambda) - 0.629\ln(d/\lambda) \qquad (10)$$

B. Ray Optics After the Hill

To model the signal at the rooftops on the flat terrain following the hill in terms of creeping rays, we make use of (6) keeping only the first term for the fields above the flat terrain after the hill, as shown in Figure 3.

The numerical and ray optical results obtained using the first term in (6) are shown in Figure 4. We have used the value of ψ taken from (14) and selected a value of D_1 to match the numerical results when the launch angle is fixed at 1.7°. Because this coefficient is determined by fitting the ray optics solution to the numerical integration results at a point close to the base of the hill, the ray optical predictions deviate by a few dB from the numerical result at greater distances. It is believed that had more terms been included in (6), the results would more closely match.

The variation of D_1 with R_h,, d, and λ can be approximated by the formula

$$\ln(D_1) = 3.14 + (0.19 + 0.031\ln(d/\lambda))\ln(R_h/\lambda) - 0.79\ln(d/\lambda) \qquad (11)$$

The magnitude of the coefficients $D_p^{m,e}$ in (6) for a smooth cylinder are significantly larger than those given by (11).

V. Sinusoidal Hills - Shape Sensitivity

Figure 6 *(a)* illustrates the path profile for a sinusoidal varying terrain, where the cylinder of Figure 3 approximately fits the first peak of Figure 6 *(a)*. Figure 6 *(b)* shows the numerical results for this profile. The minimum field strength value does not correspond to the trough of the terrain profile at 1500 m, but rather at the inflection point of the terrain preceding the trough. This behavior is consistent with the creeping ray interpretation, since the field at the terrain minimum is due to a ray that is launched from a point further up the hill, and therefore has experienced less exponential loss then at the inflection point. Also, the second maximum of the field strength does not correspond to second peak of the terrain profile, but rather occurs before this point as a result of diffraction by the previous screens. After the second peak the field strength again decreases linearly, as was previously described.

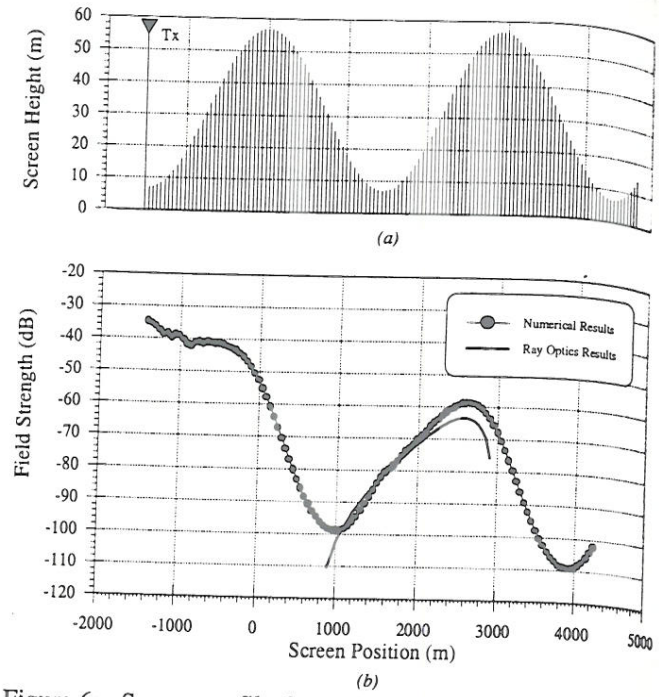

Figure 6: Screen profile for a sinusoid-like terrain path (a), and (b) the field strength predictions using the numerical and ray optics approach.

Figure 6 *(b)* shows the ray optics results for some of the screens between the first and second peaks indicated in Figure 6 *(a)*. In order to do this we replace the first peak by a cylinder to determine the creeping ray loss, and then use the local angle determined by the terrain to find $Q(\alpha)$. The result of using this method for screens near to the top of the second peak unfortunately is overly pessimistic for two reasons. First, the screens near the second peak are in the transition region about the shadow boundary from the first peak, and therefore more terms are needed in (6). Secondly, at the top of the hill (2) is unusable because α approaches zero. The results match closely on the second slope, but the ray optics predictions are pessimistic near the trough where the approximation for $Q(\alpha)$ is again inaccurate due to the small local angle. However, the creeping ray approximation is sufficiently accurate for wireless system planning at locations on the up-slope of the shadowed hill.

Figure 7 shows the screens of a trapezoidal profile, and the field strength at the top of the screens. From the transmitter at 0m to the screen at 1000m, there is no significant change in the field. From 1000m to 2000m, where the screens are at the same height as the transmitter, the field strength falls approximately as $1/\sqrt{\pi N}$. This is due to the fact that since the source is 1000m from the first screen the field incident upon the first screen looks like a plane wave. The results of [2] indicate that the field degrades as $\sim 1/\sqrt{\pi N}$ for a plane wave incident upon uniform height screens with equal separations. After the screen at 2000m there is a $1/N$ field reduction. In this range the field can be viewed as coming from the equivalent line source at the edge at 2000 m, which is subsequently diffracted by screens of

0-7803-4320-4/98/$5.00 © 1998 IEEE

uniform height and separation, leading to the familiar *1/N* variation [2]. Finally on the flat portion of the terrain the field strength begins to increase with distance and then level off

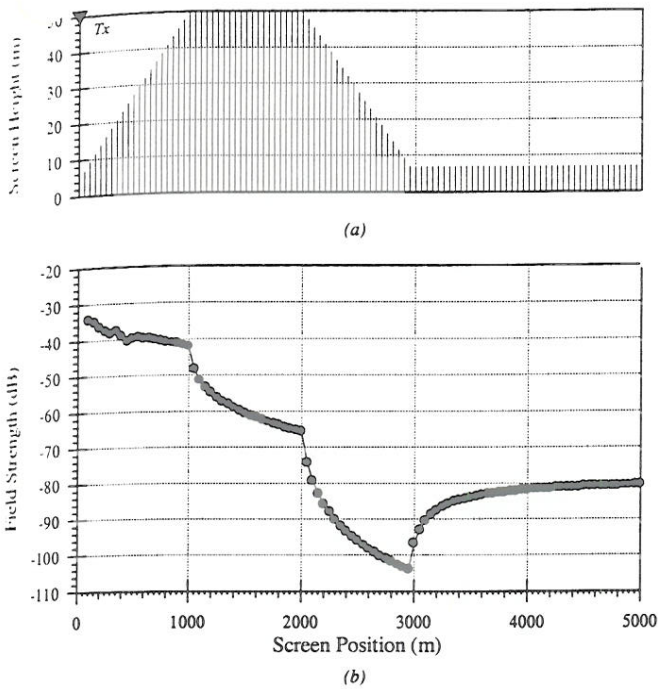

Figure 7: Screen profile for a trapezoid-like terrain path (a), and (b) the field strength predictions.

VI. Path Loss between Isotropic Antennas

For the mobile system design engineer, the efficient evaluation of path loss between isotropic antennas is of particular interest. In this regard we generalize the previous results for a line source by accounting for spreading of rays in the direction perpendicular to the plane of incidence. At points on the shadowed side of a hill, such as location ② in Figure 1, the path loss ratio between received and transmitted power is

$$P_L = \left(\frac{\lambda}{4\pi}\right)^2 \frac{e^{-2\psi\theta}}{RL_1} D_H^2 P_d \qquad (12)$$

Assuming that vertical displacements are small compared to the horizontal displacements, R is the distance from the base station to the mobile. Also, L_1 is the distance from the base station to the hill along a ray that is just tangent to the hill. The diffraction loss down to the mobile from the preceding building is given by P_d, and D_H and ψ are given by (10) and (9) for the appropriate hill radius.

For locations, such as ③ in Figure 1, that are shadowed by a previous hill, the path loss ratio is

$$P_L = \left(\frac{\lambda}{4\pi}\right)^2 \frac{e^{-2\psi\theta}}{RL_1L_2} D_I^2 Q^2(\alpha) P_d \qquad (13)$$

where R is again the distance between the base station and the mobile. Also, L_1 is as previously defined, and L_2 is the distance from the launch point on the hill to the building just before the mobile. Here $Q(\alpha)$ is the multiple diffraction loss due to the rows of houses before the mobile, and D_I is obtain from equation (11).

VII. Conclusions

This work has demonstrated that multiple diffraction past absorbing half-screens on a cylindrical path profile can be parameterized as creeping ray behavior around a cylinder. Consistent with the ray optics formulation, we have determined necessary coefficients as a function of frequency, hill radii, and screen separation. In the limit as the screen separation approaches 0, the exponential loss factor ψ approaches that of TE diffraction by a smooth cylinder. The diffraction coefficient, D_I, is significantly smaller than that given by the smooth cylinder formulations. The effects of considering houses on the terrain profile is similar to adding a roughness factor to the diffraction results for a smooth cylinder [10]. Using the fit equations given in this work the path loss over buildings located on rolling terrain may be determined.

References

[1] J. Walfisch and H.L. Bertoni, "*A Theoretical Model of UHF Propagation in Urban Environments*", IEEE Trans. on Ant. and Prop., vol. 36, no. 12, pp. 1788-1796, Dec. 1988.

[2] H.H. Xia and H.L. Bertoni, "*Diffraction of Cylindrical and Plane Waves by an Array of Absorbing Half Screens*", IEEE Trans. on Ant. and Prop., vol. 40, no. 2, pp. 170-177, 1992.

[3] S.R. Saunders and F.R. Bonar, "*Prediction of Mobile Radio Wave Propagation Over Buildings of Irregular Heights and Spacings*", IEEE Trans. on Ant. and Prop., vol. 42, no. 2, pp. 137-144, Feb. 1994.

[4] L.E. Vogler, "*An Attenuation Function for Multiple Knife-Edge Diffraction*", Radio Science, vol. 19, pp. 1541-1546, 1982.

[5] W.C.Y. Lee, "*Studies of Base-Station Antenna Height Effects on Mobile Radio*", IEEE Trans. on Veh. Tech., vol. 29, no.2, pp. 252-260, May 1980.

[6] J.B. Keller, "*Diffraction by a convex cylinder*", IEEE Trans. on Ant. and Prop., vol. 24, pp. 312-321, 1956.

[7] G.L. James, Geometrical Theory of Diffraction for Electromagnetic Waves, Peter Peregrinus Ltd., Stevenage, England, 1976.

[8] H.L. Bertoni, W. Honcharenko, L.R. Maciel, and H.H. Xia, "*UHF Propagation Prediction for Wireless Personal Communications*", IEEE Proc., Vol. 82, no. 9, pp. 1333-1359, Sept. 1994.

[9] L.R. Maciel, H.L. Bertoni, and H.H. Xia, "*Propagation Over Buildings for Paths Oblique to the Street Grid*", Proc. Int. Sym. on Personal Indoor and Mobile Radio Commun., Boston, Ma, pp. 75-79, 1992.

[10] K. Hacking, "*R.F. Propagation Over Rounded Hills*", IEE Proc., Vol. 117, no. 3, pp. 499-511, March 1970.